

A Systematic Evaluation of Object Detection Networks for Scientific Plots

Pritha Ganguly*, Nitesh Methani*, Mitesh M. Khapra, and Pratyush Kumar

Department of Computer Science and Engineering
Robert Bosch Centre for Data Science and AI (RBC-DSAI)
Indian Institute of Technology Madras, Chennai, India
{prithag,nmethani,miteshk,pratyush}@cse.iitm.ac.in

Abstract. *Are existing object detection methods adequate for detecting text and visual elements in scientific plots which are arguably different than the objects found in natural images?* To answer this question, we train and compare the accuracy of Fast/Faster R-CNN, SSD, YOLO and RetinaNet on the PlotQA dataset with over 220,000 scientific plots. At the standard IOU setting of 0.5, most networks perform well with mAP scores greater than 80% in detecting the relatively simple objects in plots. However, the performance drops drastically when evaluated at a stricter IOU of 0.9 with the best model giving a mAP of 35.70%. Note that such a stricter evaluation is essential when dealing with scientific plots where even minor localisation errors can lead to large errors in downstream numerical inferences. Given this poor performance, we propose minor modifications to existing models by combining ideas from different object detection networks. While this significantly improves the performance, there are still 2 main issues: (i) performance on text objects which are essential for reasoning is very poor, and (ii) inference time is unacceptably large considering the simplicity of plots. Based on these experiments and results, we identify the following considerations for improving object detection on plots: (a) small inference time, (b) higher precision on text objects, and (c) more accurate localisation with a custom loss function with non-negligible loss values at high IOU (> 0.8). We propose a network which meets all these considerations: It is **16x** faster than the best performing competitor and significantly improves upon the accuracy of existing models with a mAP of 93.44%@0.9 IOU.

Keywords: Computer Vision, Object Detection, Scientific Plots

1 Introduction

Object detection is one of the fundamental problems in computer vision with the aim of answering *what objects are where* in a given input image. Most of the object detection research in the past few years has been on natural images with real-life objects. For instance, in the PASCAL VOC dataset[3], the four

* The first two authors have contributed equally

major classes of objects are people, animals, vehicles, and indoor objects such as furniture. In this work, we study object detection for a very different class of images, namely computer-generated scientific plots. Fig. 1b shows an example of a scientific plot: It is a bar plot depicting the number of neonatal deaths in Bulgaria and Cuba over two years. Object detection on this plot would be required to identify different visual and textual elements of the plot such as bars, legend previews and labels for ticks, axes & legend entries. Such object detection can then enable a question-answering task. For instance, for Fig. 1b we could ask “In which year does Cuba have lower neonatal deaths?”. Clearly, this has use-cases in data analytics, and has been studied in recent research [8,9,13].

It should be clear that scientific plots differ significantly from natural images, and so does the application of object detection networks on them. Firstly, plots have a combination of textual and visual elements interspersed throughout. The text can either be very short (such as numerical tick labels) or span multiple lines (such as in plot titles). Secondly, objects in a plot have a large range of sizes and aspect ratios. Depending on the value represented, a bar in a bar-plot can be short or long, while in a line-plot a thin line would depict the data. Thirdly, plots impose structural relationships between some of the objects. For instance, the legend preview and the close-by title text denote a correspondence map. This also applies to a tick label and its corresponding bar in a bar-plot.

Given these differences, it needs to be seen if existing object detection methods are adequate for scientific plots. In particular, are they capable of (a) detecting short and long pieces of text, (b) detecting objects with large data-dependent range of sizes and aspect ratios, and (c) localising objects accurately enough to extract structural relationships between objects. To answer this question, we first evaluate state-of-the-art object detection networks on the PlotQA dataset [13] which has over 220,000 scientific plots sourced from real-world data thereby having a realistic vocabulary of axes variables and complex data patterns which mimic the plots found in scientific documents and reports. We observe that, across these models, the average of mAP@0.5 is only around 87%, indicating success in detecting the relatively simple objects in the plot.

While the above results appear positive, a closer manual inspection revealed that these models make critical errors which lead to large errors in downstream numerical inference on the plots. This disparity is because we use an IOU of 0.5 while computing the mAP scores. While IOU values in the range of 0.5 and 0.7 are acceptable for natural images where large relative areas are covered by foreground objects, such values are unacceptably low for scientific plots. This is demonstrated in Fig. 1a with two example images from the PASCAL VOC dataset where the predicted box (red) is very different from the ground truth box (cyan), but still acceptable as the IOU is within range. Contrast this with the case for the plot in Fig. 1b. For an IOU setting of 0.5 (left) and 0.75 (middle), the estimated values of the data-points would incorrectly identify that neonatal deaths in Cuba are lower in 2002 than the actual value in 2003. Only at the high IOU value of 0.9, this is correctly resolved. Thus, downstream numerical reasoning on plots requires much stricter IOU settings in comparison to object

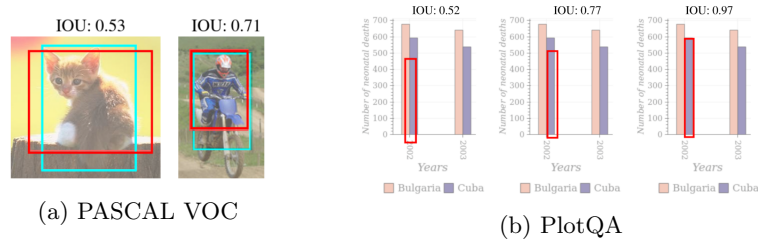


Fig. 1: Demonstrating sensitivity to IOU on images from (a) PASCAL VOC and (b) PlotQA dataset. Localising on the natural images in (a) is accurate even at low IOU thresholds of 0.5 and 0.75. For the plots in (b), the comparison of plotted values for the two years is incorrect at lower IOU values of 0.5 (left) and 0.75 (centre), and is correct for 0.9 (right).

detection on natural images. For the PlotQA dataset if we use a stricter IOU of 0.9, then the mAP scores for all models drop drastically with the best model giving a mAP of only about 35.70%. In particular, single-stage detectors such as SSD and YOLO-v3 have single digit mAP@0.9.

The poor performance of current models at high IOU settings motivate improvements in the models. We first propose minor modifications to existing models. In particular, we propose a hybrid network which combines Faster-RCNN[15] with the feature pyramid network from RetinaNet[11] and the ROIAlign idea from Mask-RCNN [6]. This significantly improves the performance and gives an overall mAP of 77.2%@0.9 IOU. However, careful analysis reveals two major limitations: (i) accuracy on text objects is very low which can lead to errors in downstream analytics tasks, and (ii) the inference time is very high (374 ms) which is unacceptable given the lower visual complexity of scientific plots. To improve the speed and performance further, we propose an architecture which contains (i) a fast and conservative region proposal method based on Laplacian edge detectors, (ii) a linking component which combines multiple region proposals for better detection of longer textual objects, and (iii) a new loss function specifically designed to improve localisation at higher IOUs. This model significantly improves accuracy with a mAP of 93.44%@0.9 IOU. Further, it is 16x faster than its closest competitor and has 3x fewer FLOPs.

In summary, the contributions of this paper are as follows:

1. We motivate the need for object detection at extreme IOU values for the specific dataset of scientific plots which require accurate localization.
2. We evaluate the robustness of 8 different object detection networks (SSD, YOLOv3, RetinaNet, variants of Fast and Faster R-CNN) to increase in IOU and identify that Feature Pyramid Network(FPN) and ROI-Align(RA) are good design choices for higher accuracy.
3. We propose PlotNet that improves on mAP by over 16 points while reducing execution time by over 16 times from its closest competitor. Thus, PlotNet is

faster than one-stage detectors and simultaneously more accurate than the best two-stage detectors.

The rest of the paper is organised as follows. We summarise the important object detection models and ideas in Section 2. In Section 3, we detail the experimental setup and the dataset. We also report results and critique the performance of different networks on the PlotQA dataset on an example plot image. In Section 4, we detail the architecture of PlotNet and in Section 5 we compare it with other networks in terms of accuracy and speed. Note that, we follow an unconventional organisation of describing partial experimental results in Section 3 as this lays the groundwork for motivating the design and evaluation of PlotNet in Section 4.

2 Existing Models for Object Detection

We now summarise the various CNN-based models and some key insights.

R-CNN [5] was the first CNN-based object detector. It uses selective search (SS) [16] which combines the best of exhaustive search and segmentation to identify about 2,000 candidate region proposals. Each region proposal is independently classified based on features extracted from the cropped region of that proposal.

Fast R-CNN [4] speeds-up R-CNN by computing the features for all proposals jointly from an intermediate layer of a CNN. It also introduced ROI Pool which warps the variable sized proposals into a fixed-size before classification and regression tasks on fully connected layers.

Faster R-CNN [15] replaced an external proposal method with a Region Proposal Network (RPN) which learns to predict proposals on pre-defined anchors of different sizes on different parts of the images.

Mask R-CNN [6] was proposed for instance segmentation and uses two stage approach for detecting and classifying objects similar to Faster R-CNN. The authors observed that ROI Pool leads to harsh quantisations of the proposed regions and hence they introduce **ROIAlign** which uses bilinear interpolation to calculate the feature map values within a scaled down size of the proposal.

Single Shot MultiBox Detector (SSD) [12] is a one-stage detector which substitutes the RPN by multiple object predictions at different pre-identified cells. These proposals are identified on feature maps of different resolutions to detect objects of different scales. This speeds up detection but at the cost of accuracy, relative to Faster R-CNN.

RetinaNet [11] uses a fixed anchor based proposal generation technique on each layer of a Feature Pyramid Network (**FPN**). FPN is a feature extractor designed for multi-scale object detection with both accuracy and speed considerations. It combines low-resolution, semantically strong features with high-resolution, semantically weak features via a top-down pathway and lateral connections. This generates a huge number ($\sim 200K$) of proposals leading to class imbalance challenge which is addressed with a custom loss function called focal loss.

YOLOv3 [14] uses bounding box priors with varying aspect ratios identified by K-means clustering on all bounding boxes in the training dataset. It addresses

the challenge of class imbalance by first predicting the probability whether the object is present and then predicting the object’s class conditional probability. In summary, single-stage detectors trade accuracy for real-time processing speed whereas two-stage detectors have higher accuracy as the proposals undergo a two-stage filtering and regression, first through RPN and then through classification and regression heads. However, these models are compute intensive as they use ResNet-50 as their feature extractor.

3 Evaluation of Existing Models

3.1 Dataset

Automated visual analysis and subsequent question-answering on scientific plots was first proposed in [9]. There are three publicly available datasets, namely FigureQA [9], DVQA [8], and PlotQA [13]. These datasets contain scientific plots with bounding boxes and labels for different plot elements including bars, lines, tick labels, legend entries, and plot labels. We run our experiments on the PlotQA dataset [13], as it is based on real-world data while both FigureQA and DVQA are based on synthetic data. For instance, in synthetic datasets, the label names are selected from a limited vocabulary such as colour names in FigureQA and top-1000 nouns in the Brown corpus in DVQA. On the other hand, PlotQA has datasets collected from public data repositories. This impacts object detection as the text labels show large variability in PlotQA dataset. Secondly, synthetic datasets use limited range of plotted values such as integers in a fixed range, while PlotQA plots real data. This impacts object detection as the size of bars in a bar-plot and the slopes in a line-plot show large variability in PlotQA dataset.

The PlotQA dataset [13] contains over 220,000 scientific plots across three categories of bar (both horizontal and vertical), line, and scatter plots. The dataset includes ground truth bounding boxes for bars, dot-lines, legend labels, legend previews, plot tile, axes ticks and their labels. The underlying data is from data sources such as World Bank Open Data, Open Government Data, *etc.* containing natural variable names such as mortality rate, crop yield, country names, and so on. The 220,000 images in the PlotQA dataset are divided to create the train (70%), validation (15%) and test (15%) splits.

3.2 Training Setup

We used the existing implementations for the R-CNN family, YOLOv3, SSD and RetinaNet. ResNet-50(R-50) pre-trained on ImageNet [2] dataset is the backbone feature extractor for Fast R-CNN, Faster R-CNN, Mask-RCNN and RetinaNet. For SSD and YOLOv3, InceptionNet and DarkNet-53 were the backbone feature extractors, respectively.

These models were trained with an initial base learning rate of 0.025 with momentum stochastic gradient descent algorithm. The network’s classification

and regression heads use a batch-size of 512 ROIs. RetinaNet and SSD models were trained with a batch size of 32 with an initial learning rate of 0.004. Based on evaluation on the validation dataset, we modified the parameters in the focal loss for RetinaNet to $\alpha = 0.75$ and $\gamma = 1.0$, against recommended values of $\alpha = 0.25$ and $\gamma = 1.0$. The model was trained with a batch-size of 64 and an initial learning rate of 0.001.

3.3 Results and Comparative Analysis

For each of the models, mAP score at three different IOU values of 0.9, 0.75, and 0.5 are shown in Table 1. In addition, for the IOU value of 0.9, we report class-wise average precision (AP). The models in the Table are sorted in increasing order of mAP@0.9. Here are the important observations:

- mAP@0.5 is fairly high (average over 87%) across models indicating that the relatively simple visual elements of the plots are being identified with high accuracy.
- mAP@0.75 falls markedly in comparison to mAP@0.5, with an average drop of about 22 points across models. Specifically for SSD, Faster R-CNN the drop is very high at about 40 points.
- mAP@0.9 drops to remarkably low values; on average mAP@0.9 is less than half of mAP@0.75. Specifically, SSD, Faster R-CNN, and YOLO have single digit mAP@0.9 values.
- For IOU of 0.9, the AP for individual classes shows large variability across models. Relatively, plot-title and dot-line classes have the lowest AP values across models.

To better illustrate the performance of each model we exemplify the bounding box outputs of the different models on specific parts of an example plot shown in Fig. 2. We make the following observations, model-wise.

- **SSD** glaringly misses detecting one of the bars, and also has low localisation accuracy as evidenced in the mis-aligned bounding for the second bar in Fig. 2a. However, it correctly detects small tick labels, perhaps due to proposal generation performed at multiple resolutions.
- **YOLOv3** detects all objects (including both bars), but with lower localisation accuracy. For instance in Fig. 2b, the upper bar and plot title have misaligned bounding boxes. To see if this problem could have been solved by imposing priors on aspect ratios of bounding boxes, we plotted aspect ratios of all objects across plots and found no distinct clusters, i.e., aspect ratios of bars, texts, *etc.* vary in a continuum. This makes it hard to choose appropriate priors for bounding boxes.
- **RetinaNet** which is based on SSD also misses out on detecting one of the bars and also the y-tick label (Fig. 2c). The bounding box of the detected bar is more accurate than that in SSD, perhaps indicating the benefit of the lateral connections in generating features for the regression head. Across the

Table 1: Comparison of existing object detection models on the PlotQA dataset with mAP scores (in %) at IOUs of 0.9, 0.75, and 0.5. For IOU at 0.9, the class-wise average precision (in %) is shown for respective classes: (a) bars, (b) dot-lines, (c) legend-labels, (d) legend-previews, (e) plot-title, (f) x-axis labels, (g) x-axis ticks, (h) y-axis labels, and (i) y-axis ticks.

IOU	0.9										0.75	0.5
Class\ Models	(a)	(b)	(c)	(d)	(e)	(f)	(g)	(h)	(i)	mAP	mAP	mAP
SSD	1.39	0.6	2.18	0.39	0.04	3.39	0.44	5.14	0.2	1.53	39.78	82.33
Yolo-v3	15.51	8.72	7.15	11.70	0.02	4.39	8.08	9.59	1.70	7.43	73.31	96.27
RetinaNet	16.51	18.5	77.26	29.74	16.58	67.62	28.40	3.14	17.31	30.56	81.13	90.13
FRCNN	53.38	1.68	12.59	14.06	0.03	42.13	25.49	11.68	31.98	21.45	63.68	72.83
FrRCNN	6.92	1.68	1.39	1.45	0.00	4.35	6.10	3.57	5.18	4.08	50.51	88.49
Mask RCNN	47.54	5.36	50.83	32.43	0.33	40.20	33.72	80.53	30.31	35.70	82.45	93.72

three single-stage detectors, which have much higher speed than the two-stage detectors, RetinaNet is the clear winner. While not apparent in the illustrated example, RetinaNet’s focal loss with custom tuned parameters (α, β) instead of hard suppression, may also be contributing to its higher performance.

- **Fast R-CNN** (FRCNN) breaks up one of the bars into smaller objects (aligning with lines on the background grid of the plot). It also misses several objects including a legend item, the plot title, and a tick label (Fig. 2d). This could be attributed to the proposal generation method which uses selective search (SS). This under-performance is also visible at low IOUs: mAP@0.5 is lowest for Fast R-CNN potentially due to poorly performing SS which remains unaffected by IOU.
- **Faster R-CNN** (FrRCNN) improves over the recall of SS by detecting most objects due to more complex region proposal network (RPN). However, RPN creates multiple overlapping proposals, even after non-maximal suppression (NMS) (Fig. 2e). This lowers this bulky model’s mAP to just 4, which is second-lowest.
- **Mask RCNN** uses Faster-RCNN as the backbone architecture but uses ROIAlign instead of ROIPool gives mixed results when compared to Faster-RCNN. It is able to detect the longer textual elements (e.g., title) but has poorer localisation accuracy on the bars. It also breaks up one of the bars into smaller objects. However, its localisation accuracy on the tick labels is better than Faster-RCNN.

In summary, most state-of-the-art models have low robustness to high IOU values on this different class of images.

3.4 A hybrid network combining existing ideas

The above discussion clearly establishes the need for better models for object detection over scientific plots. However, before we do so, we wanted to examine

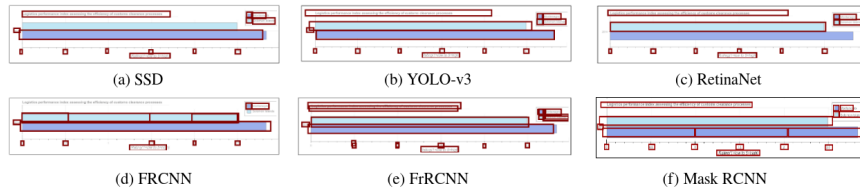


Fig. 2: Detected bounding boxes on an example plot from PlotQA dataset for different models corresponding to Table 1 at IOU 0.9.

Table 2: Comparison of modified models on the PlotQA dataset with mAP scores (in %) at IOUs of 0.9, 0.75, and 0.5. For IOU@0.9, the class-wise average precision (in %) is shown for classes as defined in Table 1.

IOU	0.9										0.75	0.5
Class\ Models	(a)	(b)	(c)	(d)	(e)	(f)	(g)	(h)	(i)	mAP	mAP	mAP
FRCNN (FPN+RA)	87.59	31.62	79.05	66.39	0.22	69.78	88.29	46.63	84.60	61.57	69.82	72.18
FrRCNN (RA)	63.89	14.79	70.95	60.61	0.18	83.89	60.76	93.47	50.87	55.49	89.14	96.8
FrRCNN (FPN+RA)	85.54	27.86	93.68	96.30	0.22	99.09	96.04	99.46	96.80	77.22	94.58	97.76

if combining ideas from existing models can help in improving the performance. Among the single-stage detectors, RetinaNet gave the best performance. Similarly, among the two-stage detectors Mask-RCNN gave the best performance. However, the qualitative analysis presented in Fig. 2 suggested that Faster-RCNN has some advantages over Mask-RCNN. Taking all of this into consideration we decided to combine the relative merits of Faster-RCNN, RetinaNet and Mask-RCNN. In particular, we retain the overall architecture of Faster-RCNN but use FPN as the feature extractor (as in RetinaNet) and replace ROI Pool with ROI Align (as in Mask-RCNN). The results obtained by making these modifications are summarised in Table 2. For the sake of completeness we also present results obtained by combining Fast-RCNN (FRCNN) with FPN and ROI Align. We observe that across all three IOU values, the highest mAP values are obtained by Faster R-CNN with FPN and ROI Align. This mAP of 77.22% is significantly better than the best number reported in Table 1.

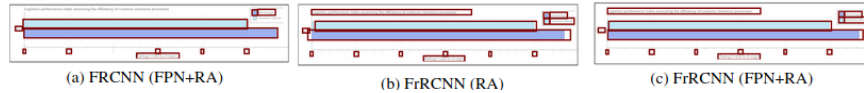


Fig. 3: Detected bounding boxes on an example plot from PlotQA dataset for different models corresponding to Table 2 at IOU 0.9.

We also do the same qualitative analysis as before for the three models presented in Table 2 and make the following observations (see Fig. 3).

- **Fast R-CNN with FPN and ROIAAlign** (FRCNN (FPN+RA)) improves on Fast-RCNN by not breaking up the bar into smaller objects, due to the FPN which enables improved feature extraction for the regression head. However due to the use of Selective Search (SS), many objects continue to go undetected (Fig. 3a). Notably, for the detected objects, the localisation accuracy is high, perhaps due to the use of ROIAAlign’s bilinear interpolation when mapping proposals into smaller cells.
- **Faster R-CNN with ROIAAlign** (FrRCNN (RA)) improves on Faster-RCNN due to the substitution of ROI Pool with ROIAAlign. This leads to more accurate localisation and thereby removal of multiple proposals by NMS (Fig. 3b). Interestingly, this model under-performs Fast R-CNN with FPN and ROIAAlign as evident in the mAP values and in the example by the difference in localisation accuracy. This illustrates the importance of FPN in being able to nullify the limitations of SS and further improve localisation.
- **Faster R-CNN with FPN and ROIAAlign** (FrRCNN (FPN+RA)) performs the best amongst all existing models. It combines the RPN of Faster R-CNN for better region proposals, with FPN which provide better features, and ROIAAlign which provides better mapping of features to scaled cells (Fig. 3c). There is an additive effect of combining these three important ideas in object detection, as evidenced by the significant difference between this model and the rest.

In summary and reassuringly, the model with the highest performance is the one that combines the best ideas in object detection.

4 Our Proposed Model

Given the low mAP scores of existing models at the requisite IOU of 0.9, we propose a new network (shown in Fig. 4) which is designed bottom up based on three key observations. First, we observe that networks which use existing region proposal methods such as selective search, RPN, and anchor based methods have low mAP@0.9. In particular, these methods either generate too many proposals or miss out some objects. We contrast this with the apparent low visual complexity of these plots which suggests that detecting region proposals should be easier. Based on this insight, we propose a region proposal method which relies on traditional CV-based methods such as edge detection followed by contour detection. We however retain ROIAAlign and FPN components which improved the performance of models. However, we note that FPN adds a significant computational cost and its addition needs to be carefully evaluated. While doing so, we make our second observation that longer textual elements such as titles and preview labels get detected as multiple proposals which need to be linked. We propose a separate linking component which decides whether a given proposal needs to be merged with any of its neighbors. None of the existing

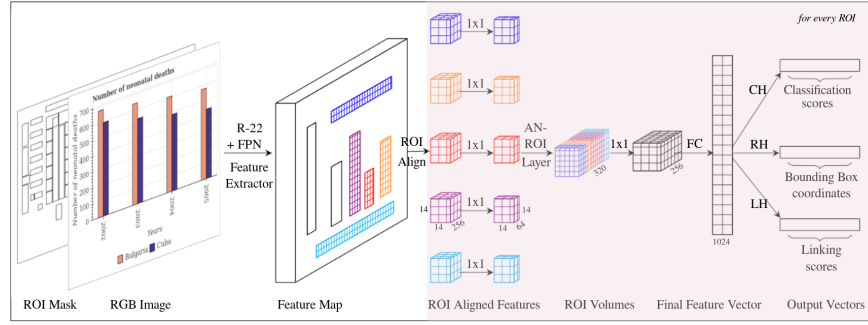


Fig. 4: Architecture diagram of our proposed model, PlotNet.

models perform such linking. Third, we notice the sharp decline of mAP scores on increase in the IOU. To address this we design a custom loss function, which has non-negligible loss values for high IOU such as greater than 0.8.

In summary, in the design of a custom model which we refer to as PlotNet, we (i) use a computationally efficient CV-based region proposal method, (ii) supplement it with a link prediction method to detect contiguous text objects, (iii) use ROIAlign to better map proposals into smaller cells, (iv) evaluate the necessity of FPN, and (v) evaluate the need for custom loss functions. In the following paragraphs, we describe different components of our model.

Region Proposal: As an alternative to Region Proposal Network (RPN), we propose a combination of CV methods to generate region proposals (Fig. 5(a)). Specifically, we (a) draw edges with a Laplacian edge detector on the image of the plot, (b) extract continuous closed contours from edges based on uniform color and/or intensity, (c) convert contours to a bounding-box by finding the minimal up-right bounding rectangle for each of the identified contours.

These boxes serve as regions of interest (ROI) which are passed as input to the network. These proposals are very small in number (90 proposals on an average) in comparison to selective search which gives around $2k$ proposals. Further, while selective search takes $\sim 6740\text{ms}$ per image on average to generate proposals, our method takes only 34ms.

Feature Extraction: We use ResNet [7] for extracting features from the input image which is resized to 650×650 before being fed to the network. To exploit structural information present in the image, we add the ROIs proposed earlier as the fourth channel to the RGB input image. We tried different number of layers in the ResNet model & found that even with 10 layers we were able to get a good performance. We also consider FPN as the feature extractor with ResNet-22 as the backbone architecture as a potential trade-off between performance and cost. Once the image features are extracted, the externally generated ROIs are projected onto the feature map. To extract a fixed sized ROI feature, we pass them through the ROIAlign layer [6] which outputs the fixed size feature map of size $14 \times 14 \times 256$. We further reduce the depth of each ROI feature map to $14 \times 14 \times 64$ by using 1×1 convolution layers.

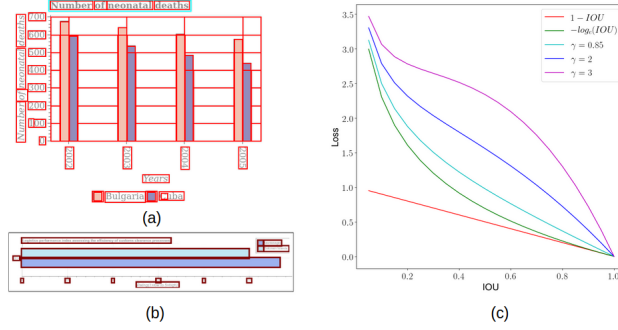


Fig. 5: (a) The proposals generated by our CV method are shown in red. (b) Detected bounding boxes by PlotNet-v7 on an example plot from PlotQA dataset at IOU 0.9. (c) Comparison of different loss functions at varying IOUs.

Accumulating Neighbouring ROI Information(AN-ROI layer): To incorporate local neighbouring information into each ROI feature, we create an AN-ROI volume by concatenating the ROI’s immediate left, right, top and bottom features along the depth, resulting in a feature volume of size $14 \times 14 \times 320$. We then apply convolutional layers on this AN-ROI volume resulting in a feature volume of size $14 \times 14 \times 256$. We hypothesise that such neighbour features would increase the accuracy of classifying, regressing, or linking individual ROIs.

Classification(CH), Regression(RH) and Linking heads(LH): The ROI features extracted above are passed through two fully-connected layers with 2048 and 1024 neurons respectively. Each ROI feature vector, is independently passed through the CH which uses the softmax function to output a probability distribution over the 9 classes of objects in the images and a tenth background class. These 9 classes are bar, dot-line, legend-preview, legend-label, plot-title, x-axis label, y-axis label, x-axis ticks and y-axis ticks. The same ROI feature vector is also fed to the RH which predicts the 4 co-ordinates (top-left and bottom-right) of the bounding box. Lastly, the same ROI feature vector is passed to the LH which predicts whether this ROI needs to be merged with none, one, or more of its immediate 4 (top, left, right and bottom) neighbours.

4.1 Custom Loss function

Most state-of-the-art object detection models use ℓ_n loss (e.g., ℓ_2 -loss, smooth ℓ_1 -loss) for performing bounding box regression. However, several studies[17][1] suggest that there are some disadvantages of doing so and instead an IOU based loss function which better correlates with the final evaluation metric should be used. Indeed, some studies have showed that using $-\log IOU$ [17] and $1 - IOU$ [1] as loss function gives better results by ensuring that (i) the training objective is aligned with the evaluation metric and, (ii) all the 4 coordinates of the bounding box are considered jointly. However, as shown in Fig. 5(c), these loss functions

have negligible values if the IOU between the predicted box and the ground truth box is reasonably high (say, > 0.8). As mentioned earlier, while this is acceptable for objects in natural images it is not suitable for objects in scientific plots which require stricter localisation. To account for this, we propose a custom loss function which give non-negligible values at high IOUs as shown in Fig. 5(c). Mathematically, the loss is defined by the following function:

$$\mathcal{L} = -(1 + IOU)^\gamma * \log(IOU)$$

The hyperparameter γ determines the rate of the scaling factor. We have experimented with a couple of γ values and have found experimentally that $\gamma = 2$ works best for PlotQA dataset.

4.2 Training and Implementation Details

While training, for every proposed ROI, we need to assign a ground-truth class for the 9 object classes and the background class. We identify the ROI’s center and identify if it lies in any of the ground-truth bounding boxes. There would be at most one such box, since objects in plots do not overlap unlike natural images. If no such ground truth bounding box is found, the ROI is considered to be in the background class and is ignored by the regression head.

Similarly, for every proposed ROI, the coordinates of the parent ground-truth box identified above are assigned as the regression targets. In particular, for visual ROIs, the regression target is set to the co-ordinates of the parent box. For textual objects, it is difficult to regress the ROI to match the entire span of the parent box. For example, in Fig. 5(a), for the ROI containing the word “Number” in the title, the ground truth box would be the entire title spanning all the words (cyan box). To avoid this large difference from the proposal, we create the regression targets for “Number” by clipping the ground-truth box to have the same boundary as the proposed box along the horizontal direction. The task then is to just grow the proposed ROI in the vertical direction and then later link it to its neighbor thereby creating the entire title box.

Lastly, for creating the ground-truth for linking, we assign a binary value to each ROI for each of the 4 directions. These 4 values indicate whether the ROI needs to be linked to its left, right, top, or bottom neighbors. In order to find the neighbours, we consider an area of 50×50 around a ROI and check if any of the neighbouring ROIs have the same parent box. If so, we assign 1 to the link corresponding to the direction (top, right, bottom, left) of that neighbour.

We trained our model for 10 epochs using Adam optimizer [10] with initial learning rate of 0.0001. We used the smooth L1-loss for bounding box regression and cross-entropy loss for classification as well as link prediction.

5 Discussion

We now discuss the performance of the following variants of our model:

Table 3: Comparison of variants of PlotNet on the PlotQA dataset with mAP scores (in %) at IOUs of 0.9, 0.75, and 0.5. For IOU at 0.9, the class-wise average precision (in %) is shown for classes as defined in Table 1.

IOU	0.9										0.75	0.5
Class\ Model	(a)	(b)	(c)	(d)	(e)	(f)	(g)	(h)	(i)	mAP	mAP	mAP
v0	91.02	31.69	97.08	81.57	99.36	96.06	85.33	82.00	90.95	83.89	97.21	98.11
v1	92.16	61.18	98.38	93.46	99.44	97.21	94.21	95.45	94.42	91.77	97.74	98.24
v2	91.79	41.86	93.74	94.64	98.29	83.11	85.69	89.32	49.36	80.87	96.38	98.20
v3	91.83	45.78	91.48	94.15	98.95	74.24	87.19	89.34	50.11	80.34	96.97	98.26
v4	91.88	61.44	96.44	95.58	99.27	97.19	90.64	97.55	87.66	90.88	97.30	98.31
v5	92.78	68.26	97.75	95.90	99.04	93.64	92.97	96.24	93.12	92.19	97.70	98.18
v6	92.74	59.12	94.87	95.58	92.46	94.46	94.12	95.36	76.85	88.39	96.78	97.82
v7	92.80	70.11	98.47	96.33	99.52	97.31	94.29	97.66	94.48	93.44	97.93	98.32

- (a) PlotNet-v0: without AN-ROI and using only the standard smooth- $L1$ loss
- (b) PlotNet-v1: with AN-ROI and using only the standard smooth- $L1$ loss
- (c) PlotNet-v2: with AN-ROI and using only $1 - IoU$ as the loss
- (d) PlotNet-v3: with AN-ROI and using only $-\log IoU$ as the loss
- (e) PlotNet-v4: with AN-ROI and using our custom loss as loss
- (f) PlotNet-v5: with AN-ROI and using smooth- $L1 + 1 - IoU$ as the loss
- (g) PlotNet-v6: with AN-ROI and using smooth- $L1 + -\log IoU$ as the loss
- (h) PlotNet-v7: with AN-ROI and using smooth- $L1 +$ our custom loss

Note that all the variants use FPN as we always get better results with FPN. We make the following observations:

Ablation Studies: Comparing the first two rows of Table 3, we observe that adding neighborhood information using AN-ROI leads to a significant improvement in the performance. Rows 3,4 and 5 suggest that when we only use one of the IOU based loss functions (without smooth-L1) the mAP@0.9 is lower than obtained using the smooth L1 loss. However, among the IOU based loss functions, our custom loss gives the best performance. Further, when combine our custom loss with the smooth L1 loss (last row) we get the best performance with an overall mAP@0.9 IOU of 93.44.

PlotNet performs better than all existing methods at all IOUs. In particular, at a strict IOU of 0.9, PlotNet improves upon its closest competitor by 16.22 absolute points. We also refer to Fig. 5(b) which shows that PlotNet detects accurate bounding boxes. We note that this example is representative of the overall performance. Amongst individual classes, PlotNet majorly improves the accuracy on plot titles which have long texts. We attribute this to combining simple region proposals with an explicit linking method. The improved accuracy of PlotNet on small objects like dot-line can be attributed to the additional neighbouring information present in each ROI feature.

Comparison to other models: In Fig. 6, we compare the mAP evaluated at 0.9 IOU and inference time of different methods. We observe that PlotNet

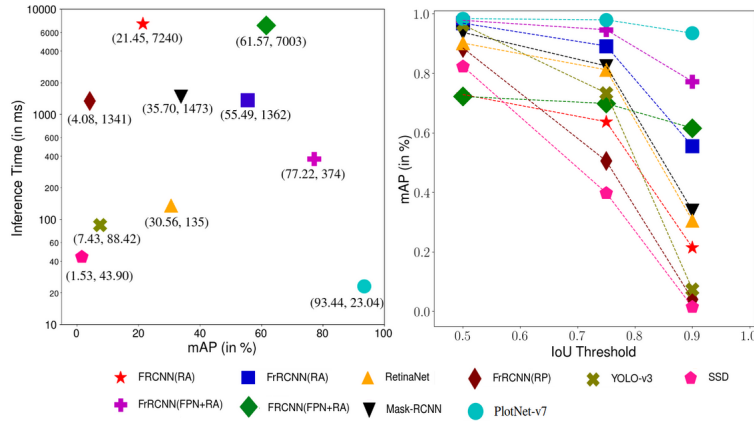


Fig. 6: Left: mAP@0.9 (in %) v/s Inference Time per image (in ms). (x, y) represents the tuple (mAP, time). Right: IOU Threshold v/s mAP (in %) for different object detection models on PlotQA.

lies in the most favorable regime, i.e., high mAP and low latency. In particular, PlotNet has the smallest inference time, beating single stage detectors. Further, it improves upon its closest competitor which is the 2-stage hybrid network (FrRCNN + FPN + ROIAlign) by 16.22 absolute points in mAP. We also refer to Fig. 5(b) which shows that PlotNet detects accurate bounding boxes. We note that this example is representative of the overall performance. Amongst individual classes, PlotNet majorly improves the accuracy on plot titles which have long texts. We attribute this to combining simple region proposals with an explicit linking method. The improved accuracy of PlotNet on small objects such as dot-line can be attributed to the additional neighbouring information present in each ROI feature.

Importance of Linking: The main motivation for introducing linking was to handle longer textual elements such as titles. Having such a mechanism allows us to work with simple region proposals and regress them to a very small delta to match the parent box in only one direction; the regression along the second direction can be taken care of by linking, one step at a time. From Table 3, we observe that this indeed works well.

6 Conclusion

We investigate the problem of detecting objects from scientific plots, which require significantly accurate localisation than objects in natural images. We first evaluate existing methods for this task and observe that while they perform well at an IOU of 0.5, the performance drops significantly at higher IOUs. We exemplified the results of different models to provide intuition for this reduced

performance. To improve the performance while not compromising on speed, we propose a new model gives an improvement of 16.22 points in mAP@0.9 when compared to its closest competitor which is a hybrid model combining the best ideas of object detection. Lastly, PlotNet’s inference time is better than all models, including single-stage detectors.

References

1. Berman, M., Triki, A.R., Blaschko, M.B.: The lovász-softmax loss: A tractable surrogate for the optimization of the intersection-over-union measure in neural networks. In: 2018 IEEE Conference on Computer Vision and Pattern Recognition, CVPR 2018, Salt Lake City, UT, USA, June 18-22, 2018. pp. 4413–4421. IEEE Computer Society (2018). <https://doi.org/10.1109/CVPR.2018.00464>
2. Deng, J., Dong, W., Socher, R., Li, L., Li, K., Li, F.: Imagenet: A large-scale hierarchical image database. In: 2009 IEEE Computer Society Conference on Computer Vision and Pattern Recognition (CVPR 2009), 20-25 June 2009, Miami, Florida, USA. pp. 248–255 (2009). <https://doi.org/10.1109/CVPRW.2009.5206848>, <https://doi.org/10.1109/CVPRW.2009.5206848>
3. Everingham, M., Van Gool, L., Williams, C.K.I., Winn, J., Zisserman, A.: The pascal visual object classes (voc) challenge. *International Journal of Computer Vision* **88**(2), 303–338 (Jun 2010). <https://doi.org/10.1007/s11263-009-0275-4>, <https://doi.org/10.1007/s11263-009-0275-4>
4. Girshick, R.B.: Fast R-CNN. In: 2015 IEEE International Conference on Computer Vision, ICCV 2015, Santiago, Chile, December 7-13, 2015. pp. 1440–1448 (2015). <https://doi.org/10.1109/ICCV.2015.169>, <https://doi.org/10.1109/ICCV.2015.169>
5. Girshick, R.B., Donahue, J., Darrell, T., Malik, J.: Rich feature hierarchies for accurate object detection and semantic segmentation. In: 2014 IEEE Conference on Computer Vision and Pattern Recognition, CVPR 2014, Columbus, OH, USA, June 23-28, 2014. pp. 580–587 (2014). <https://doi.org/10.1109/CVPR.2014.81>, <https://doi.org/10.1109/CVPR.2014.81>
6. He, K., Gkioxari, G., Dollár, P., Girshick, R.B.: Mask R-CNN. In: IEEE International Conference on Computer Vision, ICCV 2017, Venice, Italy, October 22-29, 2017. pp. 2980–2988 (2017). <https://doi.org/10.1109/ICCV.2017.322>, <https://doi.org/10.1109/ICCV.2017.322>
7. He, K., Zhang, X., Ren, S., Sun, J.: Deep residual learning for image recognition. In: 2016 IEEE Conference on Computer Vision and Pattern Recognition, CVPR 2016, Las Vegas, NV, USA, June 27-30, 2016. pp. 770–778 (2016). <https://doi.org/10.1109/CVPR.2016.90>, <https://doi.org/10.1109/CVPR.2016.90>
8. Kafle, K., Price, B.L., Cohen, S., Kanan, C.: DVQA: understanding data visualizations via question answering. In: 2018 IEEE Conference on Computer Vision and Pattern Recognition, CVPR 2018, Salt Lake City, UT, USA, June 18-22, 2018. pp. 5648–5656 (2018). <https://doi.org/10.1109/CVPR.2018.00592>
9. Kahou, S.E., Michalski, V., Atkinson, A., Kádár, Á., Trischler, A., Bengio, Y.: Figureqa: An annotated figure dataset for visual reasoning. In: 6th International Conference on Learning Representations, ICLR 2018, Vancouver, BC, Canada, April 30 - May 3, 2018, Workshop Track Proceedings (2018), <https://openreview.net/forum?id=H1mz00yDz>
10. Kingma, D., Ba, J.: Adam: A method for stochastic optimization. *International Conference on Learning Representations* (12 2014)
11. Lin, T., Goyal, P., Girshick, R.B., He, K., Dollár, P.: Focal loss for dense object detection. In: IEEE International Conference on Computer Vision, ICCV 2017, Venice, Italy, October 22-29, 2017. pp. 2999–3007 (2017). <https://doi.org/10.1109/ICCV.2017.324>, <https://doi.org/10.1109/ICCV.2017.324>

12. Liu, W., Anguelov, D., Erhan, D., Szegedy, C., Reed, S.E., Fu, C., Berg, A.C.: SSD: single shot multibox detector. In: Computer Vision - ECCV 2016 - 14th European Conference, Amsterdam, The Netherlands, October 11-14, 2016, Proceedings, Part I. pp. 21–37 (2016). https://doi.org/10.1007/978-3-319-46448-0_2, https://doi.org/10.1007/978-3-319-46448-0_2
13. Methani, N., Ganguly, P., Khapra, M.M., Kumar, P.: Plotqa: Reasoning over scientific plots. In: IEEE Winter Conference on Applications of Computer Vision, WACV 2020, Snowmass Village, CO, USA, March 1-5, 2020. pp. 1516–1525. IEEE (2020). <https://doi.org/10.1109/WACV45572.2020.9093523>, <https://doi.org/10.1109/WACV45572.2020.9093523>
14. Redmon, J., Farhadi, A.: Yolov3: An incremental improvement. CoRR **abs/1804.02767** (2018), <http://arxiv.org/abs/1804.02767>
15. Ren, S., He, K., Girshick, R.B., Sun, J.: Faster R-CNN: towards real-time object detection with region proposal networks. In: Advances in Neural Information Processing Systems 28: Annual Conference on Neural Information Processing Systems 2015, December 7-12, 2015, Montreal, Quebec, Canada. pp. 91–99 (2015), <http://papers.nips.cc/paper/5638-faster-r-cnn-towards-real-time-object-detection-with-region-proposal-networks>
16. Uijlings, J.R.R., van de Sande, K.E.A., Gevers, T., Smeulders, A.W.M.: Selective search for object recognition. International Journal of Computer Vision **104**(2), 154–171 (2013). <https://doi.org/10.1007/s11263-013-0620-5>, <https://doi.org/10.1007/s11263-013-0620-5>
17. Yu, J., Jiang, Y., Wang, Z., Cao, Z., Huang, T.S.: Unitbox: An advanced object detection network. In: Hanjalic, A., Snoek, C., Worring, M., Bulterman, D.C.A., Huet, B., Kelliher, A., Kompatsiaris, Y., Li, J. (eds.) Proceedings of the 2016 ACM Conference on Multimedia Conference, MM 2016, Amsterdam, The Netherlands, October 15-19, 2016. pp. 516–520. ACM (2016). <https://doi.org/10.1145/2964284.2967274>